20th Australasian Fluid Mechanics Conference
Perth, Australia
5-8 December 2016

# Experimental Measurements of a Self-Similar Adverse Pressure Gradient Turbulent Boundary Layer

**C. Atkinson**[1], **A-J. Buchner**[1], **A. Sekimoto**[1], **V. Kitsios**[1] **and J. Soria**[1,2]

[1]Laboratory for Turbulence Research in Aerospace and Combustion, Department of Mechanical and Aerospace Engineering, Monash University, Clayton 3800, Australia

[2]Department of Aeronautical Engineering
King Abdulaziz University, Jeddah, Kingdom of Saudi Arabia

**Abstract**

The structure and dynamics of adverse pressure gradient turbulent boundary layers (APG-TBL) have a significant role in the efficiency and performance of a range of transportation and energy generation platforms. This is particularly true in regions of strong adverse streamwise pressure gradient, such as near the trailing edges of wings and turbine blades, where separation of the boundary layer can significantly reduce performance with the potential for catastrophic consequences. The optimal design of such systems remains suboptimal due to a lack of fundamental understanding of how the pressure gradient influences the complex structure of the turbulent boundary layer, as illustrated by our inability to adequately scale the statistical flow quantities with varying pressure gradient.

To enable an investigation of both the spatially and temporally coherent structure of APG-TBLs, a series of high-speed particle image velocimetry measurements were performed in a large water tunnel with a flexible and fully adjustable roof in order to allow for the adjustment of streamwise pressure gradient. Results show a significant departure from the more widely studied zero pressure gradient flow as a significant proportion of the turbulent activity moves out to a position roughly one displacement thickness above the wall, forming an outer turbulent fluctuation peak. The results show good agreement with DNS of a self-similar APG-TBL.

## Introduction

Separating flows, and flows on the verge of separation, are of great interest to a broad range of applications. The structure and dynamics of turbulent boundary layer flows nearing separation under the influence of a strong streamwise adverse pressure gradient is however poorly understood. The classical scaling applied to zero pressure gradient turbulent boundary layers (ZPG-TBLs), which relies on the friction velocity $u_\tau$, becomes irrelevant as streamwise pressure gradient, $dP/dx$, is increased and wall-bounded flows approach separation. Additionally, the mean streamwise velocity ceases to asymptote toward a constant freestream velocity with respect to a wall based coordinate frame.

The study of pressure gradient effects is further complicated by flow history, wherein the structure of the flow is not purely dependent on the local pressure gradient but rather maintains a signature of upstream flow history. Adverse pressure gradients are often a result of surface curvature, and it therefore becomes difficult to separate out the effect of curvature history from that of the local pressure gradient. Self-similar APG-TBLs overcome these limitations due to the collapse of all their relevant dynamical properties when normalized by the appropriate local velocity and length scales. This allows for the study of the influence of a single non-dimensional pressure gradient over the coherent domain of the boundary layer, assuming a sufficiently large self-similar domain can be established.

A turbulent boundary layer approaching the verge of separation is of particular interest as it enables us to explore the nature of the flow as it approaches the state we wish to avoid, but from a theoretical point of view also represents the only wall-bounded flow which is governed by a single velocity and length scale. The self-similarity of TBLs has received considerable theoretical assessment [14, 10], and numerous definitions have been formulated for self-similar or equilibrium TBLs. Following George and Castillo [6] and Castillo and George [4], an APG-TBL is self-similar when each term in the governing equations maintains the same proportionality with streamwise location, $x$, with each self-similar variable expressed as

$$\begin{aligned}
\langle U\rangle(x,y) &= U_e(x)\left(1-f(\zeta)\right),\\
\langle uu\rangle(x,y) &= R_{uu}(x)\, r_{uu}(\zeta),\\
\langle vv\rangle(x,y) &= R_{vv}(x)\, r_{vv}(\zeta),\\
\langle uv\rangle(x,y) &= R_{uv}(x)\, r_{uv}(\zeta),
\end{aligned} \tag{1}$$

where $U_e$ is the velocity of the local external flow, and $R_{uu}$, $R_{vv}$, and $R_{uv}$ are the Reynolds stresses. $f(\zeta)$, $r_{uu}(\zeta)$, $r_{vv}(\zeta)$, and $r_{uv}(\zeta)$ are self-similar functions of the similarity variable, $\zeta$. The momentum equation in the boundary layer can then be expressed in self-similar form [7] as

$$\begin{aligned}
&\frac{2}{K}\Lambda(x)\, f(\zeta)+\Lambda(x)\, f^2(\zeta)\\
&\qquad -\frac{1}{K}\left[\Lambda(x)-1\right]\zeta f'(\zeta)\\
&\qquad -\left[\Lambda(x)-1\right]F(\zeta)\, f'(\zeta)\\
&\qquad =C_{vv}(x)\, r'_{vv}(\zeta)\,\zeta - C_{uu}(x)\, r'_{uu}(\zeta)\,\zeta\\
&\qquad -KC_{uv}(x)\, r'_{uv}(\zeta) - D_{vv}(x)\, r_{vv}(\zeta)\\
&\qquad +D_{uu}(x)\, r_{uu}(\zeta) - K^2 C_{\nu}(x)\, f''(\zeta)
\end{aligned} \tag{2}$$

with the coefficients defined as

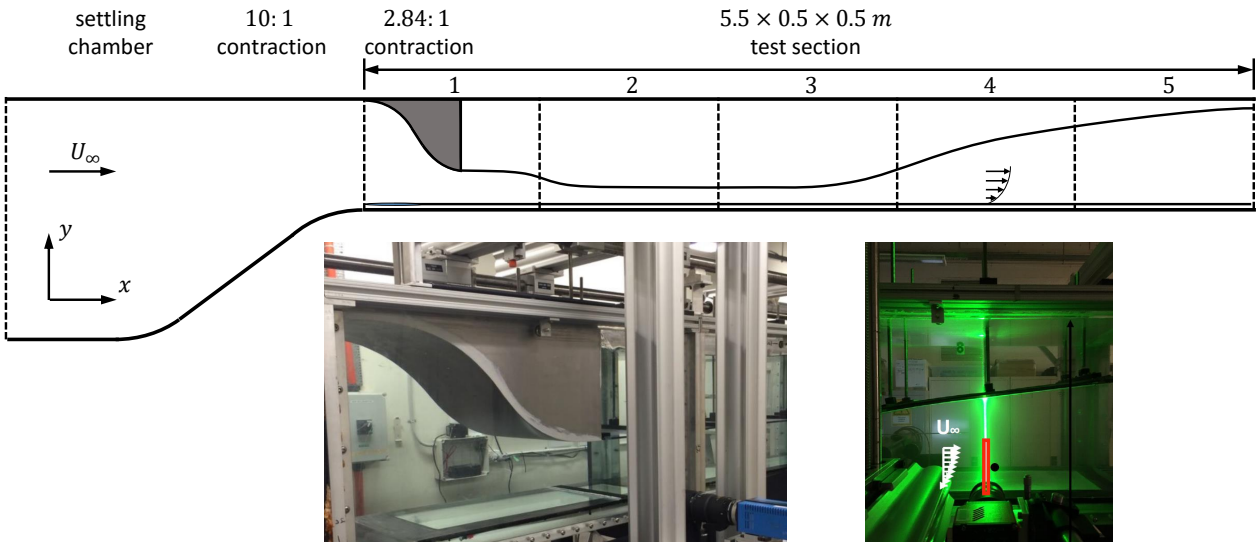


Figure 1: Schematic of the LTRAC water tunnel. Photographs are provided of the modified contraction stage, and an indicative measurement domain in the fourth test section.

$$
\begin{aligned}
\Lambda(x) &= -\delta_1 U_e \frac{dU_e}{dx} \Big/ \left( U_e^2 \frac{d\delta_1}{dx} \right), \\
C_{uu}(x) &= R_{uu}/U_e^2, \\
C_{vv}(x) &= R_{vv}/U_e^2, \\
C_{uv}(x) &= R_{uv} \Big/ \left( U_e^2 \frac{d\delta_1}{dx} \right), \\
D_{uu}(x) &= \frac{dR_{uu}}{dx} \delta_1 \Big/ \left( U_e^2 \frac{d\delta_1}{dx} \right), \\
D_{vv}(x) &= \frac{dR_{vv}}{dx} \delta_1 \Big/ \left( U_e^2 \frac{d\delta_1}{dx} \right), \\
C_\nu(x) &= -\nu \Big/ \left( U_e \delta_1 \frac{d\delta_1}{dx} \right).
\end{aligned}
\tag{3}
$$

The appropriate length and velocity scales for this flow have been shown to be $\delta_1$ and $U_e$. This comes from a more detailed and general analysis of the self-similarity condition which can be found in Kitsios *et al.* [7]. Each term in equations 3 must have the same proportionality in $x$ for the flow to be self-similar, but it can be shown that if $\Lambda$, $C_{uu}$ and $C_{vv}$ are independent of $x$ then $D_{uu}$ and $D_{vv}$ must also be independent of $x$. For the flow to be completely self-similar it is therefore only necessary that $\Lambda$, $C_{uu}$, $C_{vv}$, $C_{uv}$ and $C_\nu$ each be independent of $x$. $C_\nu$ however cannot be held independent of $x$, resulting in a viscous scaling in the inner region and a separate self-similar scaling in the outer region, in the same manner as for a ZPG-TBL. Naturally the extent of the viscous dominated inner region decreases with vanishing skin friction as the flow approaches the verge of separation. A TBL at the verge of separation is therefore the only flow that is entirely self-similar with a single length and velocity scale acting over its entire wall-normal extent.

The body of work on self-similar APG-TBLs is relatively slim when compared to that covering ZPG-TBLs and more generalised configurations acted upon by an adverse pressure gradient. Most studies focus on measurements of statistical profiles at varying streamwise positions, with varying levels of success at collapsing these profiles with appropriate scaling [13, 10, 11, 2, 3, 1]. Of these, only Stratford [13] reported a case of zero skin friction. These previous studies show that as the pressure gradient is increased, a second peak in the magnitude of the Reynolds stress components forms and becomes dominant at a wall-normal location of around $y \approx \delta_1$. This is considerably further out than the location of the near-wall peak observed for the ZPG-TBL. Direct Numerical Simulations (DNS) of self-similar APG-TBL have been performed by Skote *et al.* [12] and Lee and Sung [9] with moderate non-dimensional pressure gradients $\beta = 0.24, 0.65$ for the former and $\beta = 1.68$, defined by Clauser [5] as

$$
\beta(x) = \frac{\delta_1}{\tau_w} \frac{dP}{dx}. \tag{4}
$$

Recently Kitsios *et al.* [7, 8] undertook two large APG-TBL DNS simulations using a far field wall-normal velocity boundary condition to achieve self-similar flows on a flat surface with $\beta = 1.0$ and one at the verge of separation ($\beta \to \infty$), completely overwhelming the near-wall peak and drastically changing the shape of the mean profile. In this present work we aim to establish a self-similar APG in a large horizontal water tunnel to complement the DNS of Kitsios *et al.* [7, 8]. This paper details the methodology by which the required flow condition was achieved and presents an initial assessment of the turbulent statistics in the self-similar region.

## Experiment

Experiments were undertaken in the $500 \times 500mm$ test section water tunnel at the Laboratory for Turbulence Research in Aerospace and Combustion (LTRAC). This facility was modified by the insertion of an extra contraction at the upstream end of the test section, as well as a flexible polycarbonate roof which stretched the remaining length of the $5.5m$ test section. This roof insert could be raised or lowered via a series of threaded supporting rods, thus forming a variable area test section. Additionally, a false floor was constructed of glass and anodised aluminium and was inserted into the test section to provide a consistently flat surface upon which to perform the boundary layer measurements free of any curvature effects. This experimental arrangement is illustrated in figure 1.

The flexible roof was set so as to establish a self similar ad-

verse pressure gradient turbulent boundary layer. It was found that the greatest Reynolds number could be achieved, with the lowest freestream turbulence, by further contracting the flow downstream of the contraction insert. A reduced test section cross-section of $500 \times 132mm$ was maintained over a streamwise distance of approximately $x = 2700mm$ before the cross section was rapidly expanded from the beginning of the fourth test section. Test measurements indicated that within this reduced cross-section portion of the tunnel, the turbulent boundary layers over the false floor and roof inserts remained distinct and separate.

Accurate prediction of the roof profile required to establish the desired APG-TBL is confounded by the need to account for the growing boundary layers on all four walls of the test section, as well as corner effects. As such, it was necessary to iteratively adjust the roof position using the accelerated PIV analysis approach described in Atkinson *et al.* [3, 1]. This procedure involves measuring the boundary layer at multiple streamwise locations and processing the images in real time using an in-house image acquisition and PIV analysis algorithm. The near-instantaneous provision of statistics using this approach allows for rapid adjustment of the roof to the desired position.

It was found during testing that initial flow separation occurs in this facility on the flexible roof, rather than the floor. For this reason, a self-similar TBL on the lower floor was established under a moderate adverse pressure gradient in the fourth test section. The mean freestream velocity in the self similar region was approximately $440 - 470mm/s$.

An ILA sCMOS camera was controlled using an in-house code to record images directly to memory. To localise the measurement and to speed up image acquisition, the camera was operated with a reduced sensor size of $2560 \times 96$ pixels, allowing an image acquisition rate of up to $790Hz$. Acquiring single exposure images with a rapid shutter speed allowed the use of an Oxxius Slim $226mW$ continuous-wave laser operating at $532nm$ wavelength. The laser was spread into a $1mm$ thick, $12mm$ wide lightsheet. The exposure time of $500\mu s$ yielded an apparent particle image diameter of between 2 and 3 pixels. Imaging was performed using a $50mm$ Zeiss Makro-Planar lens with $f_\# = 2.8$. The flow was seeded with $11\mu m$ diameter Potters hollow glass spheres (specific gravity $\gamma = 1.1$).

| | |
|---|---|
| Magnification | $M = 0.14$ |
| Spatial resolution | 21.1 $pixels/mm$ |
| Lens aperture | $f_\# = 2.8$ |
| light sheet thickness | $\Delta z \approx 1mm$ |
| field of view | $8.35 \times 167mm$ |
| interframe time | $\Delta t = 1.5ms$ |
| interrogation window size | $96 \times 64$ *pixel* (first pass), $32 \times 32$ *pixel* (second pass) |

Table 1: Parameters for APG-TBL Measurements.

Of course in the present case it is not sufficient to merely rapidly acquire these particle images, but rather we also need the resulting velocity statistics at a fast rate. Images were acquired in batch mode and were then spread across the six processors present in the lab computer (Intel Xeon e5620 $2.40GHz$) with the program collating the computed velocity fields before acquiring the next batch of images. Statistics were computed and plotted once a predefined number of image batches had been recorded. The maximum rate at which these velocity fields can be acquired is obviously a function of the number of processors, the image size and the size and overlap of the interrogation windows desired. The parameters used for the present investigation are shown in table 1, resulting in vector fields of $5 \times 159$ vectors recorded and processed at just under $25Hz$.

#### Results

The properties of the APG-TBL were measured over a range of streamwise locations, from $x = 3.68$ to $x = 4.18m$. At each location 5000 independent batches, each consisting of 6 instantaneous velocity fields, were acquired. After averaging in the streamwise dimension, the statistics each y-location were calculated from a total of $150,000$ samples.

The wall-normal profiles of the mean streamwise velocity, $U$, and the three Reynolds stress components, $\langle uu \rangle$, $\langle vv \rangle$, and $\langle uv \rangle$, are shown in figure 2. Profiles are given for six streamwise locations between $x = 3.68 - 4.18m$ at intervals differing by $100mm$, and all values are normalised by the outer velocity and the displacement thickness.

As was the case for the measurements presented by Atkinson *et al.* [1] of the roof boundary layer, the collapse of the mean streamwise velocity profile is good. Unlike the roof boundary layer measurements however, which showed a trend towards increasing fluctuating velocity magnitudes with streamwise position, the collapse of the Reynolds stress profiles in these measurements is also almost complete. All three Reynolds stress components display a peak at a position just above $y = \delta_1$, matching with the DNS results of Kitsios *et al.* [7] for $\beta \approx 1$. The magnitude of the outer Reynolds stress peaks are measured as approximately $\langle uu \rangle = 0.01U_e^2$, $\langle vv \rangle = 0.0035U_e^2$, and $\langle uv \rangle = 0.0024U_e^2$, comparing favourably to the Reynolds stress peak magnitudes suggested from the DNS of Kitsios *et al.* [7]. The measurements extend down to approximately $y/\delta_1 = 0.25$ from the wall, which is sufficient to observe some indication of the formation of an inner peak in the $\langle uu \rangle$ profile. Measurements aimed at quantifying this peak under the current experimental conditions are ongoing.

As expected for an APG-TBL at constant $\beta$, the boundary layer thickness increases linearly with $x$. Figure 3 shows the streamwise variation of the Reynolds number in the self-similar region, based on both displacement thickness, $\delta_1$ and momentum thickness $\delta_2$. The approximate range of values of each are $5600 \leq Re_{\delta_1} \leq 7800$ and $2600 \leq Re_{\delta_2} \leq 4000$, respectively.

#### Conclusions

A high-speed PIV velocity profiling system was created using an ILA sCMOS camera coupled with a continuous-wave laser. This system enabled close to real-time assessment of boundary layer statistics at multiple streamwise locations, and subsequent rapid iterative adjustment of the experimental facility to achieve the desired flow conditions. In the present experiment this system was used to guide the adjustment of a flexible roof in a large water tunnel and subsequently enable the establishment of an adverse pressure gradient turbulent boundary layer at the verge of separation.

A self-similar moderate APG was established over a streamwise domain of $9\delta$ with $Re_{\delta_1} = 5600$ to 7800 and $\beta \approx 1.4$. The resulting mean velocity and Reynolds stress profiles compare closely with previous DNS simulations and collapse when scaled with the outer velocity and displacement thickness. The outer turbulent fluctuation peak is well resolved and measurements are currently underway to resolve the near wall region and quantify the wall shear stress.

#### Acknowledgements

The authors would like to acknowledge the research funding from the Australian Research Council. Julio Soria gratefully acknowledges the support of an Australian Research Council

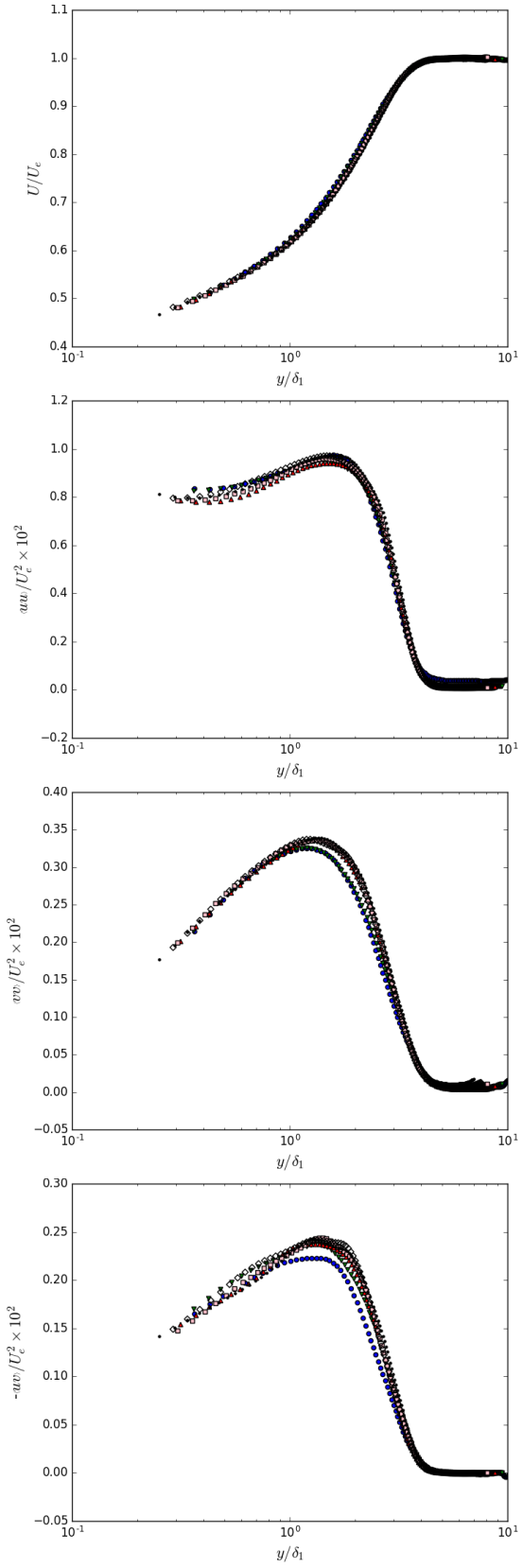


Figure 2: Wall-normal profiles of mean streamwise velocity and the Reynolds stresses. Data are presented for six locations between $x = 3.68 - 4.18m$.

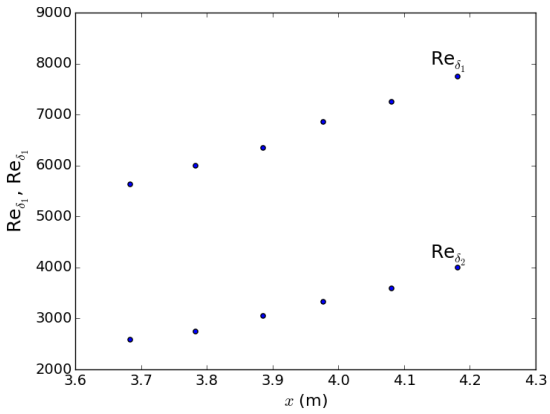


Figure 3: Reynolds number based on displacement thickness and momentum thickness at each streamwise measurement location.

Discovery Outstanding Researcher Award fellowship and Callum Atkinson an Australian Research Council Discovery Early Career Researcher Award fellowship.

### References

[1] Atkinson C., Buchner A-J., Eisfelder M., Kitsios V., Soria J., 18th Int. Sym. on App. of Laser and Imaging Techniques to Fluid Mechanics, 4–7 July 2016, Lisbon Portugal.

[2] Atkinson C., Buchner A-J., Kitsios V., Soria J., 3rd Sym. on Fluid-Structure-Sound Interaction and Control, 5–9 July 2015, Perth Australia.

[3] Atkinson C., Buchner A-J., Kitsios V., Soria J. (2015b) 11th Int. Sym. on Particle Image Velocimetry - PIV15, 14–16 September 2015, Santa Barbara California.

[4] Castillo L., George W.K. (2001) AIAA Journal 39 (1), 41-47.

[5] Clauser, F. (1954) J. Aero. Sci. 21, 91–108.

[6] George W.K., Castillo L. (1993) Near-wall Turbulent Flows, pp. 901-910.

[7] Kitsios V., Atkinson C., Sillero J.A., Borrell G., Gungor A.G., Jiménez J., Soria J. (2016a) Int. J. of Heat and Fluid Flow, in press.

[8] Kitsios V., Atkinson C., Sillero J.A., Borrell G., Gungor A.G., Jiménez J., Soria J. (2016b) Advances in Computation, Modelling and Control of Transitional and Turbulent Flows, 269-278.

[9] Lee J-H., Sung J. (2008) Int. J. Heat Fluid Flow 29, 568-578.

[10] Mellor G., Gibson D. (1966) J. Fluid. Mech. 24, 225-253.

[11] Skåre P., Krogstad P-A. (1994) J. Fluid. Mech. 272, 319-348.

[12] Skote M., Henningson D., Henkes R. (1998) Flow Turb. Combust. 60, 47-85.

[13] Stratford B. (1959) J. Fluid Mech. 8, 143-155.

[14] Townsend A. (1956) The structure of turbulent shear flow, Cambridge University Press.

[15] Willert C.E. (2015) Exp. Fluids 56 (17).